Available online at www.sciencedirect.com
SCIENCE DIRECT®
ELSEVIER
Journal of Non-Crystalline Solids 328 (2003) 123–136
JOURNAL OF NON-CRYSTALLINE SOLIDS
www.elsevier.com/locate/jnoncrysol

X-ray absorption spectroscopy analysis of formation and structure of Ag nanoparticles in soda-lime silicate glass

X.C. Yang [a], M. Dubiel [a,*], S. Brunsch [a], H. Hofmeister [b]

[a] Department of Physics, Martin-Luther University of Halle-Wittenberg, Friedemann-Bach-Platz 6, D-06108 Halle, Germany
[b] Max Planck Institute of Microstructure Physics, Weinberg 2, D-06120 Halle, Germany

Received 20 December 2002; received in revised form 24 March 2003

Abstract

Ag nanoparticles of 2.8–7 nm mean size were fabricated in soda-lime glass of varying iron oxide content by Na^+/Ag^+ ion exchange and subsequent thermal treatment. Fe^{2+} ions have been identified as reducing agent for Ag ions by analysis of the X-ray absorption near edge structure at the Fe K-edge and of the extended X-ray absorption fine structure (EXAFS) at the Ag K-edge. EXAFS analysis accompanied by electron microscopy investigation has shown that crystalline Ag particles in glass with high content of iron oxide (0.865% Fe_2O_3) exhibit a lattice dilatation. Furthermore, the calculated data demonstrate that with decreasing particle size lattice disorder and anharmonic effects, and hence also the thermal expansion coefficient, increase. This size effect is more distinctly pronounced for glass samples of reduced thickness as well as upon gradual thermal treatment applied for particle preparation. The results indicate substantial influence of the surrounding glass matrix on formation, structure and thermodynamic properties of Ag particles.

PACS: 61.10.–I; 61.16.–d; 61.46.+w; 61.43.–j

1. Introduction

Silicate glass containing metal nanoparticles was investigated in the previous century mainly because of the specific optical absorption (see for example [1–3]). Recently, the preparation and characterization of such composites has been further stimulated by peculiar non-linear optical properties, especially an increased third-order susceptibility, making such glass a promising candidate for application in integrated optics and photonics [4–6]. Previous studies indicated that the optical properties of nanoparticle/glass composites strongly depend on the morphology, mean size, size distribution and concentration of the embedded nanoparticles as well as their interaction with the host matrix [7–9]. Therefore, different preparation methods like ion implantation [10,11], ion exchange [12,13], reducing atmosphere treatment [14], ion irradiation [15,16], electron irradiation [17], laser irradiation [18], co-sputtering of

* Corresponding author. Tel.: +49-345 5525 524; fax: +49-345 5527 159.
E-mail address: dubiel@physik.uni-halle.de (M. Dubiel).

0022-3093/$ - see front matter © 2003 Elsevier B.V. All rights reserved.
doi:10.1016/S0022-3093(03)00469-1

metal–glass targets [19] and sol–gel technique [20] have been used to fabricate specific configurations of nanoparticles in glasses. Formation and structural characteristics of nanoparticles were mainly studied by transmission electron microscopy (TEM) and high resolution electron microscopy (HREM) [21], optical absorption spectroscopy and time-resolved photoluminescence [22], Fourier transform infrared spectroscopy [23], X-ray photoelectron spectroscopy [24] and X-ray absorption spectroscopy [25–27].

Ion exchange and subsequent thermal treatment near the glass transformation temperature is an easy and efficient technique to achieve metal nanoparticle formation in glass, but the long-standing problem of the relatively broad particle size distribution restricts the application in actual devices [13]. In addition, the nature of the interaction between precipitate and glass matrix across the common interface is not well understood [28]. This is a general problem for all composite materials. Our recent investigations by HREM and extended X-ray absorption fine structure (EXAFS) spectroscopy have shown that the mechanical state of Ag nanoparticles in soda-lime glass is sensitively reflected by their structure, which allows one to draw conclusions on the process of particle formation [26,29–31]. It was found that the content of iron oxide strongly influences the concentration of precipitated particles. In addition, it could be demonstrated that the size distribution of particles as well as the spatial distribution of mean particle size in the glass are important for the interpretation of structural data determined by EXAFS spectroscopy.

Therefore, the present work is aimed at obtaining Ag nanoparticles of narrow size distribution and reduced mean particle size in glass of varying composition. That should allow a deeper insight into the interaction between the nanoparticles and glass matrix, and on the particle formation process, i.e. Ag/Na ion exchange followed by appropriate thermal processing. To this purpose, glass samples of reduced thickness have been used and a gradual thermal processing has been applied. Investigation of Ag incorporation into the glass network has been carried out by X-ray absorption spectroscopy analysis of both, XANES and EXAFS spectra. From EXAFS spectra structural information on the local environment like coordination number and species surrounding a detected atom, the interatomic distance $\boldsymbol{r}$, the mean-square relative displacement σ^2, being the so-called Debye–Waller factor, and the mean-cubic relative displacement $\boldsymbol{C}_3$ [26,32–34] have been derived. Furthermore, Debye temperature and thermal expansion coefficient (TEC) of Ag nanoparticles have been calculated from cumulant parameters of temperature-dependent EXAFS measurements [34–38]. XANES spectra have been used to extract information about valence states and coordination environment of existing Fe species [39,40]. The effect of the Fe ion content on the formation of Ag nanoparticles has been discussed based on XANES and EXAFS analyses. The Einstein temperature and TEC of Ag nanoparticles embedded in glass have been calculated and compared to previous results.

2. Experimental

Slide samples of two types of soda-lime glass of 0.16 mm thickness were prepared by grinding and polishing: glass 1, a conventional soda-lime glass containing 0.13 wt% Fe_2O_3, and glass 2, so-called green glass (Flachglas AG, Germany) containing 0.865 wt% Fe_2O_3. The respective glass composition is shown in Table 1. In all cases, the float glass surface that contains tin ions owing to the glass fabrication process has been removed by the grinding procedure before Ag doping by ion exchange. The glass slides were immersed in a molten mixture of $NaNO_3$ and 0.05 wt% $AgNO_3$ held at 330 °C for different durations. Under these conditions the Ag^+/Na^+ exchange ratio is 6%. After cooling down to room temperature (RT) the ion-exchanged samples were subjected to thermal processing in air at different temperatures for varying duration as specified in Table 2. The long duration of ion exchange and the small thickness of the slides should enable a homogeneous distribution of Ag species throughout the glass. While Ag nanoparticle formation in samples 1a–1c and 2c was induced by a single annealing, a two-step annealing procedure was applied to samples 2a

Table 1
Glass composition (in wt%)

Glass	SiO_2	Na_2O	CaO	MgO	Al_2O_3	K_2O	BaO	TiO_2	SO_3	Fe_2O_3
1	72.6	14.37	6.18	4.06	1.54	0.64	–	–	0.4	0.13
2	71.87	13.3	8.69	4.15	0.59	0.31	0.01	0.079	0.148	0.865

Table 2
Preparation conditions

Sample	Ion exchange	Annealing	
	Duration (h)	Temperature (°C)	Duration (h)
1a	310	–	–
1b	310	480	120
1c	310	600	168
2a	382	380	432
		600	97
2b	429	380	810
		480	384
2c	426	410	459

and 2b to achieve a more narrow Ag particle size distribution. Conventional TEM by means of a JEM 1010 operating at 100 kV was used to determine the particle size. More than 200 particles were processed to establish the particle size distribution in each case. The electron optical magnification used was 50 000 or 100 000. Application of a cross-section preparation technique allowed one to monitor the particle size variation throughout the glass.

Ag K-edge (25.514 keV) EXAFS and Fe K-edge (7.112 keV) XANES spectra were measured at beamline X1 and E4 of HASYLAB (Hamburg, Germany) in transmission mode, utilizing Si(3 1 1) and Si(1 1 1) double-crystal monochromator, respectively. The energy resolution of the experiments was $\Delta E/E \cong 2.5 \times 10^{-4}$. Harmonic rejection was achieved by detuning the monochromator crystals between 40% and 50%. While the Fe K-edge XANES spectra of the glass samples have been measured at liquid nitrogen or RT, the Ag K-edge EXAFS spectra of Ag foil and Ag-containing glass were systematically measured in the temperature range from 10 to 300 K using a liquid helium vapour flow cryostat equipped with an electric heater. The temperature was monitored by a thermocouple mounted on the sample holder. In addition to the spectra measured at the various glass samples, X-ray absorption spectra of bulk metal foils of Ag and Fe as well as of crystalline iron(II) sulphate (Fe_2SO_4) and iron(III) oxide (Fe_2O_3) were measured for reference purposes.

3. Data analysis

For analysing the Ag K-edge spectra, the program package UWXAFS 3.0 [36] was used to extract the EXAFS oscillation, $\chi(k)$, from the raw X-ray absorption. This EXAFS function $\chi(k)$, is given by

$$\chi(k) = \frac{\mu(k) - \mu_0(k)}{\Delta\mu(0)}, \tag{1}$$

where $\mu(k)$ is the X-ray absorption coefficient, $\mu_0(k)$ is the background absorption and $\Delta\mu(0)$ is the jump at the edge step. The photoelectron wave number k is defined by the relation

$$k = \sqrt{2m_e(E - E_0)/\hbar^2}, \tag{2}$$

where E is the incident photoelectron energy, E_0 is the absorption edge energy, $2\Pi\hbar = h$ is Planck's constant and m_e is the electron mass. The AUTOBK code was used to remove the background from the data obtained by X-ray absorption spectroscopy. The first derivative of the Ag foil spectrum measured at 12 K was tentatively chosen to calibrate the Ag K-edge energy. The $\chi(k)$ functions were weighted by k^2 and subsequently Fourier-transformed into the real space using a Hanning window function. The k range used for the Fourier transformation was 2.6–18.6 Å^{-1} for the Ag foil and 2.6–16 Å^{-1} for the glass samples. In the real space, the fit range is 1.6–4 Å in each case. The experimental EXAFS oscillation $\chi(k)$, and the corresponding Fourier transform FT, were fitted by means of theoretical phase and amplitude functions based on FEFF7.1 [36]. A more detailed

representation of the data evaluation can be found elsewhere [26,41].

From the fit procedure of the Ag K-edge spectra parameters were obtained that characterize the local environment of Ag^+ ions inside the glass network as well as the structure and thermal vibrations of Ag atoms in nanoparticles. These parameters include the interatomic distance r, the Debye–Waller factor σ^2, the coordination number N, and the third-order cumulant C_3 in dependence on the measuring temperature. The Debye–Waller factor represents the mean-square relative displacement of interatomic distances of neighbouring atoms. The mean-cubic relative displacement C_3 is associated with an asymmetric distribution of bond distances resulting from anharmonic vibrations which can be correlated to thermal expansion.With $r(T)$, $\sigma^2(T)$ and $C_3(T)$ the linear TEC α was calculated by using an anharmonic Einstein model and thermodynamic perturbation theory [35,37] according to

$$\alpha = \frac{C_3}{rT\sigma^2}\,\frac{3z(1+z)\ln(1/z)}{(1-z)(1+10z+z^2)} \tag{3}$$

with $z = \exp(-\Theta_E/T)$. Here $\Theta_E = \hbar\omega/k_B$ represents the Einstein temperature, with k_B being the Boltzmann constant. In the calculations C_3 was set to zero for the spectra of Ag foil measured at 12 K and was fitted for all other spectra. This approximation can be used since the thermodynamic parameter of silver foil is about 0.2×10^{-6} K^{-1} [42] at this temperature and decreases strongly for decreasing the temperature towards 0 K. That means, anharmonic vibrations and thermal expansion show a similar behaviour. For the Einstein model, the thermal expansion vanishes exponentially with decreasing temperatures. That gives not the correct temperature dependence near the zero point [37], but the resulting discrepancies can be neglected with respect to the uncertainty of calculated parameters (see Section 4.2.2). It should be noted here that the evaluation of the TEC by means of the temperature-dependent Ag–Ag distances $r(T)$ determined from the EXAFS data currently does not yield precise results because of two reasons [26,38]. At first, the precision is limited by the accuracy of the determination using the linear term in the EXAFS phase [38]. The second point is the influence of vibrational disorder perpendicular to the observed Ag-Ag pair in EXAFS analysis as proposed by several authors [43–45]. That gives temperature-dependent corrections of bond lengths which need to be calculated by theoretical models. For those reasons in the present work the anharmonic Einstein model was used to evaluate the thermal expansion of nanoparticles. The application of further experimental techniques like temperature-dependent diffraction experiments requires the examination of the accuracy for the specific case.

If there exists static structural disorder, i.e. a deviation from crystalline order in the bulk of the face centered cubic (fcc) Ag lattice, e.g., at the interface of Ag nanoparticles to the glass matrix, the experimental Debye–Waller factor of the first Ag–Ag coordination sphere can be represented as superposition of a static part σ_s^2 and a dynamic one σ_d^2 according to

$$\sigma^2 = \sigma_s^2 + \sigma_d^2. \tag{4}$$

To separate the temperature-independent contribution σ_s^2 characterizing the static disorder, and temperature-dependent Debye–Waller factor σ_d^2 describing the harmonic lattice vibrations, the modified Einstein model can be used to calculate σ_d^2 [46]:

$$\sigma_d^2 = \frac{\hbar^2}{2m_r k_B \Theta_E}\,\frac{(1+z)}{(1-z)}, \tag{5}$$

where m_r is the reduced mass of the Ag–Ag pair. Thus, besides the usual temperature dependence, the experimental Debye–Waller factor depends on σ_s^2 and Θ_E only which can be calculated by means of the above equations.

4. Results

4.1. XANES at Fe K-edge

The Fe K-edge spectra of Fe foil, $FeSO_4$ and Fe_2O_3 were measured as reference for Fe^0, Fe^{2+} and Fe^{3+}, respectively, to estimate the valence state of Fe ions in glass. The normalized XANES spectra at the Fe K-edge of $FeSO_4$, Fe_2O_3 and the glass samples 1 and 2 are shown in Fig. 1(a) and

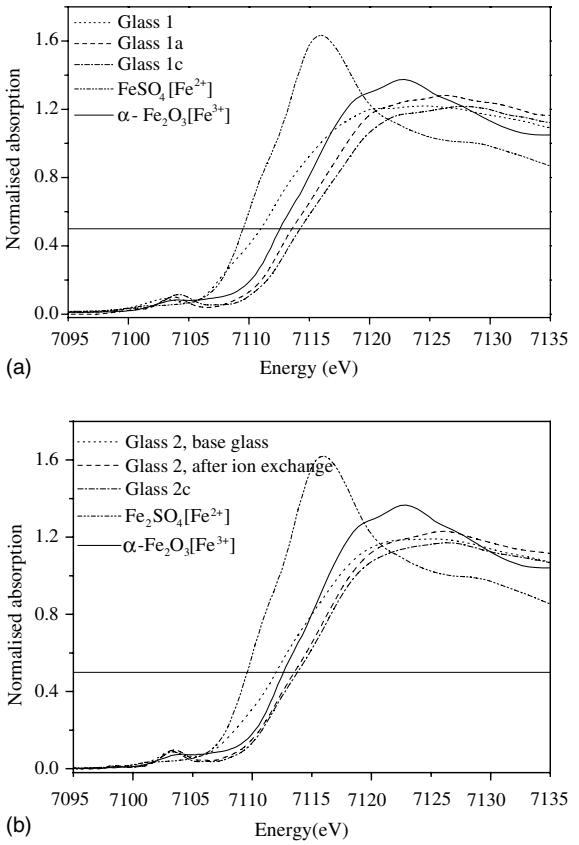

Fig. 1. Normalized Fe K-edge XANES spectra of (a) glass samples 1 and (b) glass sample 2c in the untreated, ion exchanged and annealed state, respectively, always together with the spectra of $FeSO_4$ and Fe_2O_3.

(b). Table 3 lists the Fe K-edge positions in these samples as taken at the half height of the edge. This way of recording the XANES parameter to characterize the valence state of Fe ions involved has been chosen since the reference and the glass samples exhibit rather different spectral features in both, the pre-edge and the edge region. Before being subjected to ion exchange, both glass samples, 1 and 2, exhibit a Fe K-edge position comparable to that of the reference compounds. Already after Ag doping by ion exchange they exhibit a certain shift of the Fe K-edge. Annealing near the glass transformation temperature T_G (480–600 °C) causes for both glass samples a further, but smaller shift as can be seen from Table 3.

4.2. EXAFS at Ag K-edge in glasses

4.2.1. Glass 1– conventional glass

Fig. 2 shows the Fourier-transformed EXAFS oscillations measured at the Ag K-edge of glass samples 1a–1c containing only 0.13% Fe_2O_3, upon Ag^+/Na^+ ion exchange at an exchange ratio of 6%, where 1a is the one without thermal treatment while 1b and 1c have been annealed at 480 and 600 °C, respectively. The Fourier-transformed curve represents a modified radial distribution of neighbours around an absorbing atom, i.e. the peaks reflect various coordination spheres of Ag–O, Ag–Ag and Ag–Si pair correlations. Hence, it is possible to retrieve the coordination spheres of Ag species from the spectra. Fitting, as shown for example for sample 1a, has been done by using the program FEFF 7.01. The first two peaks, marked Ag–OI and Ag–OII correspond to the first and second Ag–O coordination sphere, while the third peak marked Ag–AgI corresponds to the first Ag coordination sphere. The first Ag–O pair correlation dominates the spectra irrespective of the ion exchange ratio which has only minor effect on the peak structure. For a detailed discussion of the glass structure and the correlations of the various constituents see [47]. From Fig. 2 it becomes clear that even in the glass samples annealed at 480 and 600 °C only a slight increase of the Ag–Ag pair

Table 3
Fe–K edge position

Sample	$FeSO_4$	Fe_2O_3	Glass 1 (base glass)	Glass 1a (after ion exchange, 310 h)	Glass 1c (after annealing)	Glass 2 (base glass)	Glass 2 (after ion exchange, 426 h)	Glass 2c (after annealing)
Fe K-edge position (eV)	7109.5	7112.6	7111.0	7113.6	7114.2	7111.8	7113.4	7113.8

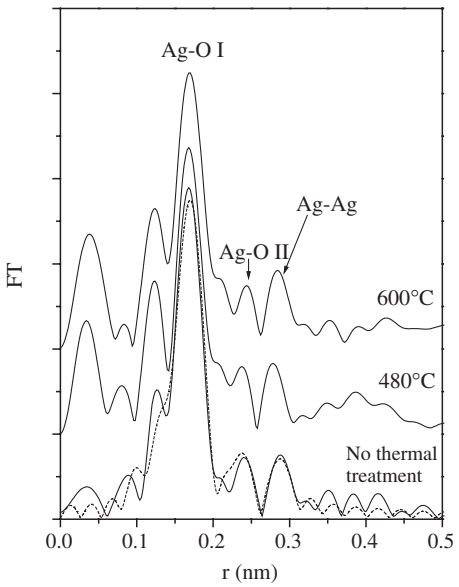

Fig. 2. Fourier transforms of Ag K-edge spectra of glass samples 1a–1c with 6% ion exchange ratio. The dotted line shows a fitted spectrum (sample 1a) calculated by FEFF 7.01.

correlation due to Ag nanoparticle formation is observed.

4.2.2. Glass 2 – green glass

The EXAFS oscillations of the Ag foil as well as glass samples 2a–2c exhibit distinct changes with temperature as it is shown in Fig. 3(a)–(d). It is quite obvious that with increasing temperature the spectra exhibit amplitude reduction and phase delay being due to the enhancement of the mean-square and cubic relative displacements. The Fourier-transformed spectra of glass samples 2a–2c for 12 K measuring temperature are shown in Fig. 4 together with curve fitting (dashed lines) by the UWXAF 3.0 program assuming Ag nanoparticle sizes of 7.0, 4.0 and 2.8 nm for glass samples 2a, 2b and 2c, respectively. These are the mean particle size values as determined by TEM. By comparing Figs. 2 and 4 it may be recognized that, in contrast to the situation of sample 1 with low Fe content, the Fourier-transformed spectra of samples 2 are clearly dominated by the Ag–Ag pair correlations owing to the distinctly larger concentration of Ag nanoparticles. The peak positions marked are quite according to those seen in Fig. 2, i.e. the first one is attributed to the first Ag–O coordination sphere, while the following 4 peaks correspond to the first up to the fourth Ag–Ag coordination spheres. This allows one to study structural and thermodynamic parameters of Ag nanoparticles by employing the fitting and model calculations as outlined above.

Structural parameters as the Ag–Ag distance r, the mean-square relative displacement σ^2, and the mean-cubic relative displacement C_3, calculated in dependence on the measuring temperature for the first Ag–Ag coordination sphere of the Ag foil and glass samples 2a–2c are shown in Fig. 5(a)–(c). The nearest neighbour distance Ag–Ag increases with increasing temperature due to thermal expansion of both, the Ag foil as well as Ag nanoparticles, but the starting point and degree of increase differ. Samples 2a and 2b exhibit larger values of r at all temperatures; however, sample 2c does not deviate much from the bulk behaviour. Thus, there is apparently an increase of the interatomic distance in samples of increasing particle size, but because of their different thermal history a direct relation cannot be concluded. Fig. 5(b) shows that the low-temperature value of the mean-square relative displacement σ^2 increases with decreasing particle size. This behaviour indicates an increasing degree of static disorder for smaller particles owing to their enhanced proportion of surface atoms which also is demonstrated by the calculated values of the static part of the Debye–Waller factor σ_s^2 shown in Table 4. While the static part of the Ag foil is zero, the static part derived for the glass samples increases considerably with decreasing mean particle size. The temperature dependence of σ^2 as described by the Einstein temperature represents the degree of dynamic disorder owing to thermal lattice vibrations. Fig. 5(c) finally shows the mean-cubic relative displacement C_3, reflecting the anharmonic vibrations of the samples in dependence on the measuring temperature. Here an increase with decreasing mean particle size may be recognized that becomes the more pronounced the higher the temperature. The parameter uncertainty of the displayed values amounts to $\Delta r = 0.0003$ nm, $\Delta\sigma^2 = 0.00001$ nm^2 and $\Delta C_3 = 2 \times 10^{-8}$ nm^3, respectively.

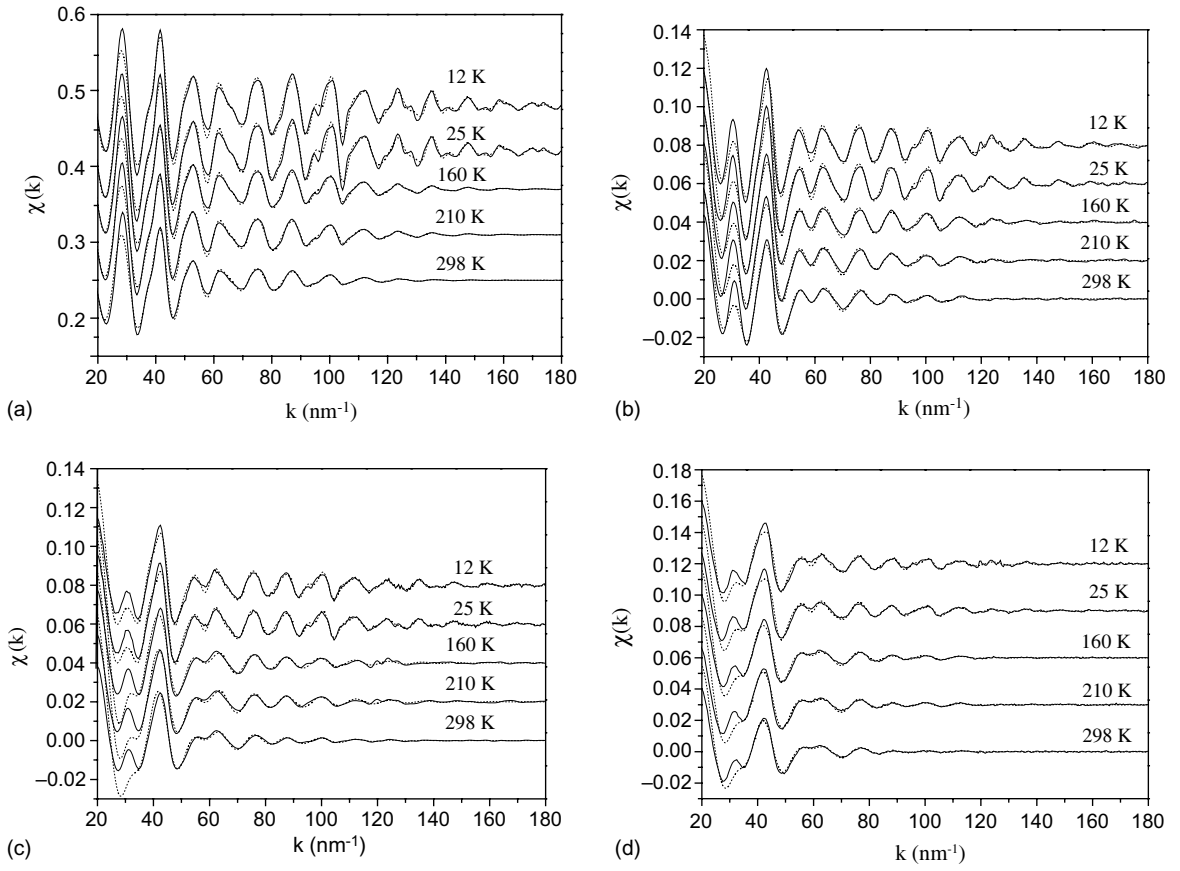

Fig. 3. Temperature dependence of the EXAFS function $\chi(T,k)$ of (a) Ag foil, (b) glass sample 2a, (c) sample 2b and (d) sample 2c together with the fitted functions (dashed lines).

Besides σ^2, Table 4 comprises also further parameters derived from the analysis of EXAFS spectra: the mean particle size and corresponding geometric standard deviation from TEM measurements, the Ag–Ag coordination number, the Einstein temperature, the Ag–O distance and Ag–O coordination number. The accuracy of the calculated Ag–Ag and Ag–O coordination numbers amounts to about 10%. The Ag–O distance has been calculated to 0.215 nm in agreement with the values obtained for glass samples containing preferentially ionic species of Ag, but the coordination numbers are distinctly smaller (1–1.5) than the reference values (2–2.5) [41,47], the larger the Ag nanoparticles in the annealed glass samples are. The coordination numbers derived from EXAFS

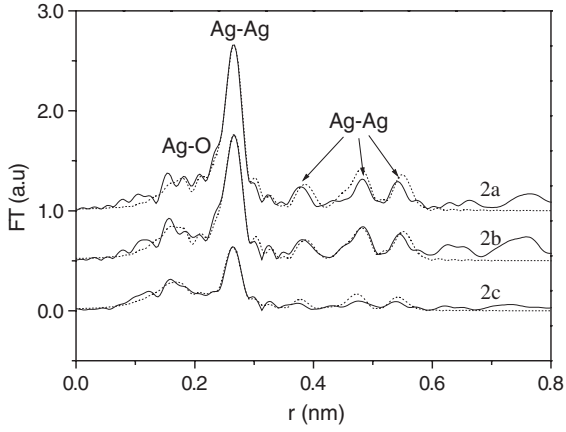

Fig. 4. Fourier transforms of the EXAFS oscillations of glass samples 2a–2c measured at 12 K and the corresponding fits (dashed lines) calculated by UWXAFS 3.0.

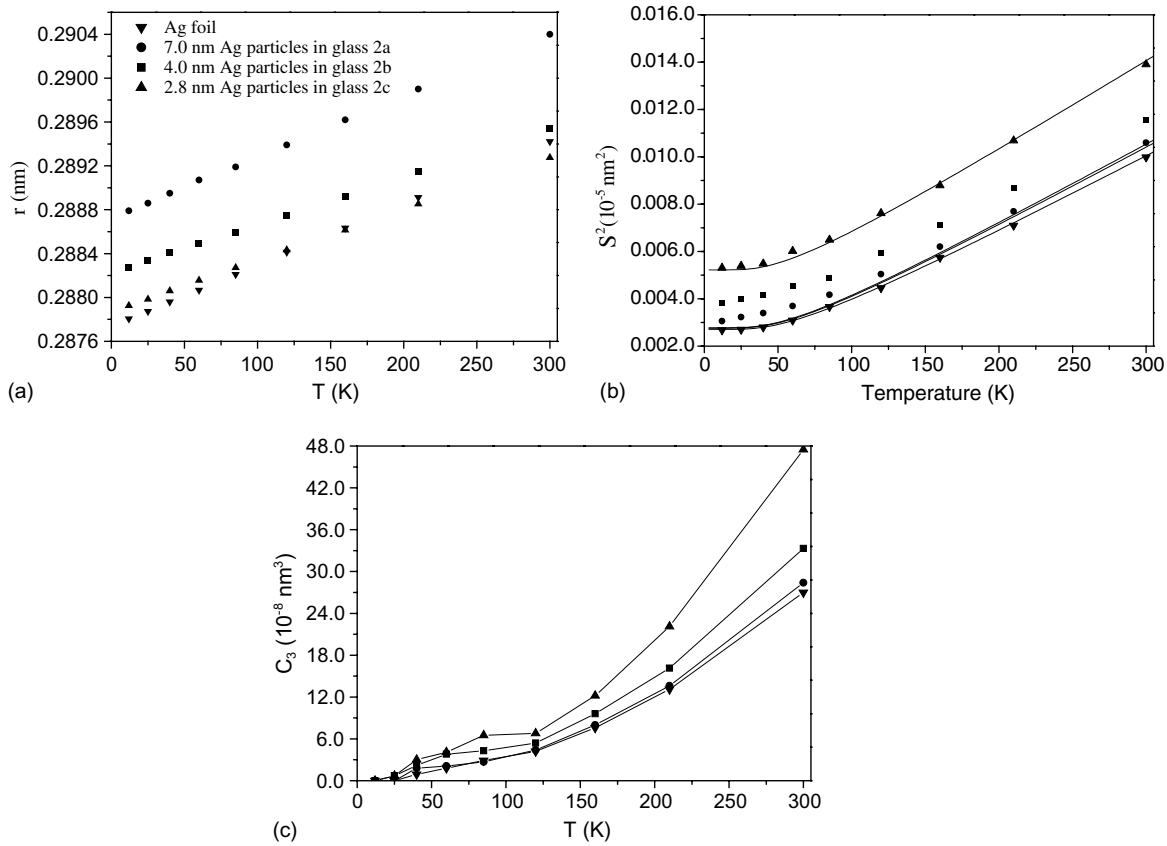

Fig. 5. Calculated structural and thermodynamic parameters of Ag foil and glass samples 2a–2c in dependence on temperature: (a) interatomic distance r, (b) mean-square relative displacement σ^2, and (c) the mean-cubic relative displacement C_3. The lines in (b) were fitted by Eqs. (4) and (5). The lines in (c) are guides for the eye.

Table 4
Particle sizes from TEM experiments and parameters from EXAFS analysis

Sample	Mean particle size d (nm)	Geometric standard deviation of d (nm)	Ag–Ag coordination number	Einstein temperature (K)	σ_s^2 (10^{-2} nm^2)	Ag–O distance (nm)	Ag–O coordination number
Ag foil	–	–	Set to 12	165	0	–	–
2a	7.0	1.35	3.8	163	0.0003	0.2150	1.0
2b	4.0	1.38	2.5	162	0.001	0.2148	1.5
2c	2.8	1.51	2.0	155	0.0025	0.2154	1.4

data must be considered as average values, which are sensitively influenced by the occurence of an oxygen-free environment of Ag species, i.e. the formation of nanoparticles. The Ag–Ag coordination number, as compared to the value of 12 for the Ag foil, has been found distinctly smaller in the glass samples because of the missing Ag–Ag coordination of ionic Ag species, which only have

oxygen environment, and because of the reduced Ag coordination of atoms situated in the particle surface. Since the proportion of surface atoms increases with decreasing size, this effect is more pronounced for smaller particles.

The temperature dependence of TEC as calculated by an anharmonic Einstein model is shown in Fig. 6 for Ag foil and the glass samples. For samples 2b and 2c with 4.0 and 2.8 nm mean particle size a considerable enhancement of TEC values by about 20–50%, in particular near RT, has been obtained. However, for the TEC values of sample 2a with 7.0 nm mean particle size nearly no change has been found within the experimental accuracy as compared to the Ag bulk value. As an example, Fig. 7 shows the size distribution with log–normal curve fit of Ag nanoparticles in sample 2c as determined by TEM. For the samples with larger particle size, i.e. 2a and 2b, the corresponding size distribution becomes narrower as a result of the two-step thermal treatment.

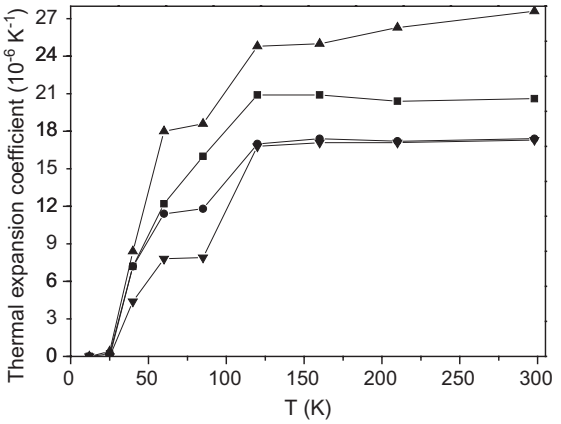

Fig. 6. Temperature dependence of calculated TEC of Ag foil and glass samples 2a–2c. The markers are the same as in Fig. 5. The lines are guides for the eye.

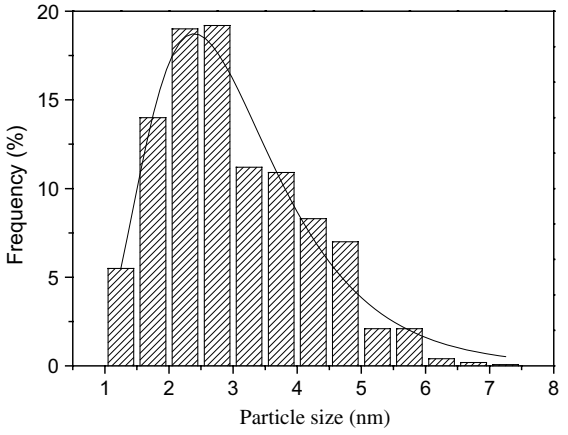

Fig. 7. Ag particle size distribution with log–normal curve fit (solid line) of glass sample 2c.

5. Discussion

5.1. Ag ion reduction and particle formation

The first step of Ag nanoparticle formation in glass being Ag doped by ion exchange is the reduction of Ag^+ ions, what may be achieved by a number of processes [48]. In our glass samples polyvalent Fe ions are considered to act as reducing agent. To confirm this process, valence state changes of Fe ions during reduction must be detected. The measured absorption spectra of Ag doped glass samples do not show detectable effects at the Ag K-edge upon thermal treatment aimed at Ag nanoparticle formation. For Fe ions, however, it is well known that the K-edge excitation energy shifts linearly with the valence state due to a changing number of screening electrons [49]. It should be mentioned here that structural changes like modifications of bond length, coordination geometry or electronegativity of neighbours may cause an additional energy shift. The Fe K-edge position of the as-received glass is comparable to that of the reference compounds in accordance with the valence state ratio Fe^{2+}/Fe^{3+} determined by optical spectroscopy of 50/50 and 26/74 for samples 1 and 2, respectively [41]. The shift of the Fe K-edge position, as observed upon Ag doping by ion exchange at 330 °C and furthermore upon Ag nanoparticle formation by annealing at temperatures between 380 °C and 600 °C, indicates that Ag^+ ion reduction by changing the Fe^{2+} ion valence state may occur during both procedures. The formation of Ag particles, that can be monitored by optical spectroscopy and electron

microscopy, is usually expected in a temperature range well above 400 °C. However, fluorescence measurements revealed thermally induced reduction of Ag^+ ions already at temperatures as low as 350 ° C for samples of glass 1 [50] and recently the formation of rather small Ag particles in samples of glass 2 has been observed just after ion exchange without annealing at higher temperatures [51]. These results and the shift of the Fe K-edge after the ion exchange demonstrate that already in this low-temperature range most of the silver ions are reduced to neutral atoms and small aggregates of silver are formed, i.e. silver clusters or nuclei of crystalline particles. Of course, these species are not visible in TEM experiments. Depending on the Ag concentration and the exchange conditions, the formation of a few detectable particles is possible as shown in [51]. Thus, we may distinguish two temperature ranges, namely, a low-temperature range of about 300–400 °C in which Ag atoms form and aggregate so as to nucleate nanoparticles, and a high-temperature range above 400 °C and around T_G in which particle growth predominates.

As can be seen from Fig. 1, the Fe K-edge position of both glass samples after ion exchange and annealing is found at higher energies than that of the Fe_2O_3 reference, although all Fe ions of the latter are in the valence state 3+. This behaviour is caused by differences in the structure of the first coordination sphere of Fe ions in both materials. The glass samples exhibit a shorter Fe–O distance and a more regular oxygen environment of Fe species than the reference [41]. Higher valence states than 3+ are not to be expected. The total shift of the Fe K-edge induced by ion exchange and Ag precipitation amounts to 3.2 eV for glass 1 and 2.0 eV for sample 2c. Considering the above mentioned valence state ratio of Fe species in both glasses and the corresponding edge positions of the reference materials one may calculate a total shift of the absorption edge due to the oxidation of Fe^{2+} to Fe^{3+} being 6.4 eV for glass 1 and 8 eV for sample 2c. These values were calculated under the assumption that after the final thermal treatment of each sample approximately all Fe ions are oxidized to the 3+ state. The data are comparable to the results of previous studies on Fe containing pyroxene ($NaFeSi_2O_6$) minerals and glass materials [39]. Hence, the reduction of Ag ions by means of Fe^{2+} may be assumed to proceed in both glass samples according to

$$Fe^{2+} + Ag^+ \rightarrow Fe^{3+} + Ag^0. \quad (6)$$

Because of the small amount of iron oxide in glass 1, even at an Ag^+/Na^+ exchange ratio of 6% the concentration of Fe^{2+} is much less than that of Ag^+. Thus, only a relatively small number of Ag particles can be formed and the Ag–O pair correlations of ionic Ag incorporated in the glass network predominate the Fourier transform of EXAFS spectra. On the other hand, the samples of glass 2 contain such a high amount of the reducing agent Fe^{2+} that a strong enhancement of the Ag particle concentration results and thus the Ag–Ag pair correlations predominate the Ag K-edge EXAFS spectra. Therefore, these samples are well suited to study the behaviour of Ag nanoparticles in glass over a broad range of temperatures by X-ray absorption spectroscopy.

5.2. Thermal expansion and lattice vibrations

Depending on the different annealing conditions the ion-exchanged samples of glass 2 contain particles of 2.8, 4.0 and 7.0 nm mean size corresponding to a ratio of the numbers of surface atoms to total atoms of 0.45, 0.33 and 0.21, respectively. As can be seen from Fig. 6 the analysis of Ag K-edge EXAFS spectra yields TEC values which distinctly deviate from the bulk value (Ag foil), in particular at temperatures above 50 K, if the mean particle size is smaller than 7 nm, or the proportion of surface atoms larger than about 20%. The calculated TEC bulk value for RT of 1.70×10^{-5} K^{-1} is consistent with reference data evaluated by thermodynamic methods [42]. The TEC of sample 2c with 2.8 nm mean particle size amounts to 2.76×10^{-5} K^{-1} at RT. This is almost the same as the one reported for a glass sample with Ag nanoparticles of 3.2 nm mean size [31], but somewhat larger than that of 2.5 nm sized particles in glass [26], both results being derived from similar EXAFS analyses. To understand this discrepancy, one must consider the width of size distribution which, besides the mean particle size,

influences sensitively the result of the analysis being of average character only. The size distribution of sample 2c exhibits a log–normal shape as shown in Fig. 7. The distribution of the 2.5 nm mean size particles [26] is distinctly broader since glass slides of 0.30 mm, instead of 0.16 mm as in the present study, have been used. The distribution of the 2.5 nm mean size particles [26] is distinctly broader since glass slides of 0.30 mm, instead of 0.16 mm as in the present study, have been used where under the conditons applied silver ions do not reach the centre of the sample. Hence, nanoparticles of quite different concentration and size are formed near the glass surface and the centre, respectively. Differences in the distribution width of particle sizes also result from variations of the thermal processing. By gradual annealing in two steps (one at 380–410 °C and a second at 480–600 °C) a more narrow size distribution of approximately Gaussian shape has been achieved for the previously studied 3.2 nm mean size particles [31] as well as for the present samples 2a and 2b as can be seen from Table 4 (cf. standard deviations). Thus, it cannot be excluded that a comparable proportion of surface atoms is present in the samples of 2.8 and 3.2 nm mean particle size what may cause a comparable deviation from the bulk value of TEC. However, this size effect appears less pronounced for wider size distributions as that of the 2.5 nm mean size particles [26].

EXAFS studies on isolated Ag nanoparticles of only 1.3 nm mean size have been reported to yield a TEC value of 10.4×10^{-5} K^{-1} [52]. This extraordinary high value most probably is caused by the even higher proportion of surface atoms of about 0.75, but also by the minor interaction to the silica substrate. Likewise, a strong influence of the particle environment has been observed for the Debye–Waller factor. The increase of σ^2 with decreasing particle size, as shown in Fig. 5(b), is mainly caused by the enhanced portion of surface atoms which is reflected by the static part σ_s^2 of the mean square relative displacement. By fitting the temperature dependence of the experimental Debye–Waller factor for the first Ag–Ag coordination sphere using a modified Einstein model, the static contribution and Einstein temperature can be separated. This static part, being zero for the Ag foil, increases with decreasing particle size (see Table 4). The temperature-dependent dynamic part σ_d^2, represented by the Einstein temperature Θ_E, characterizes the vibrational state of Ag atoms. It decreases only slightly with size for the Ag nanoparticles in samples of glass 2 from 163 K for sample 2a with 7 nm mean size to 155 K for sample 2c with 2.8 nm mean size which is 10 K below the bulk value. The asymmetric vibrations of surface atoms obviously weaken by interaction with the surrounding glass matrix. For isolated Ag nanoparticles of 1.3 nm size, however, a Debye–Waller factor increasing distinctly more with temperature and a Θ_E of only 114 K have been reported [52].

5.3. Variation of interatomic distances

The interatomic distance of samples 2a and 2b with 7.0 and 4.0 nm mean size of Ag nanoparticles, as determined by EXAFS analysis of Ag–Ag pair correlations of the first coordination sphere in dependence on the temperature, are situated distinctly above the bulk value (i.e. that of the Ag foil). Only sample 2c always exhibits values near to that of the bulk (see Fig. 5(a)). This behaviour cannot be explained by a simple relationship between particle size and interatomic distance. Deviations from the nearest-neighbour distance of the bulk fcc lattice of Ag may occur because of several reasons: (i) particle formation at elevated temperatures gives rise to stress developing during cooling down to RT because of thermal expansion mismatch of Ag and the glass matrix, (ii) small particles usually are in a size-dependent state of stress owing to their surface curvature and (iii) a modified distance is assumed on average for atoms situated at the very surface of particles since they have an incomplete or even no lattice environment.

The first contribution, uniform stress arising upon cooling to RT, is proportional to the difference in thermal expansion of glass and embedded particles [53]. With the TEC of the investigated glass being 8×10^{-6} K^{-1} at RT [54] and of the Ag nanoparticles as determined by EXAFS analysis (see Fig. 6) to 2.7×10^{-5} K^{-1} (sample 2c), 2.0×10^{-5} K^{-1} (sample 2b) and 1.72×10^{-5} K^{-1} (sample 2a), respectively, the resulting stress

clearly is tensile. Consequently, a lattice dilatation is to be expected as it has previously been found in similar green glass samples by EXAFS analysis [26,29–31]. Besides the thermal expansion mismatch, this dilatation depends on the cooling range, i.e. the difference between annealing temperature and RT. The second contribution may be described by a Laplace-type equation [55]

$$f = 3R\Delta a/2a\kappa, \tag{7}$$

where f is the surface stress or interface stress (for particles embedded in a matrix), a is the bulk lattice parameter, κ is the compressibility, a is the deviation from the bulk lattice parameter and R is the particle radius. Depending on the strength of interaction across the interface, the stress state of nanoparticles may be compressive or tensile, leading to size-dependent lattice contraction or dilatation [21,28–30]. Our recent HREM lattice analysis revealed a dilatation for Ag nanoparticles in green glass [29,30] which should be caused by several effects. The third contribution is due to edges, corners, surface steps, kinks and vacancies leading to a changed packing of surface atoms as compared to the particle interieur. This behaviour is the more pronounced the larger the proportion of surface atoms is. Very small Ag particles or clusters that contain about 100 atoms or less frequently exhibit non-crystallographic packing of atoms [56]. This characteristic can be considered as static structural disorder. However, a measurable effect should result only for extremely small particles of very small size distribution.

While the second contribution to the variation of interatomic distances clearly results in an increase or a decrease with decreasing particle size, the first one indirectly is size-dependent, since not only the cooling range is involved, but also the thermal expansion of the particles, whose size dependence has been discussed above. The interatomic distances derived from the spectra analysis, as shown in Fig. 5(a), exhibit the largest increase for sample 2a, a lesser increase for sample 2b and no distinctly pronounced increase for sample 2c. The tensile stress resulting from thermal expansion mismatch should be larger in sample 2b and even more in sample 2c than in sample 2a since the increase in thermal expansion with decreasing particle size overrides the simultaneous decrease in cooling range. This discrepancy may be attributed to size-dependent changes of the elastic behaviour of small metal particles which have not been considered here since there are no data available up to now. Furthermore, a size-dependent strength of adhesion between particles and matrix may be assumed, such that the interfacial attraction decreases with decreasing particle size. This will result in a reduced mediation of the tensile stress to smaller particles and hence lesser changes of the interatomic distance occur. Both issues need to be treated in the frame of thermoelastic modeling of the processes of stress build-up and stress relief during particle formation.

6. Conclusions

The formation of Ag nanoparticles in soda-lime glass of varying content of iron oxide, Ag doped by ion exchange at 330 °C, upon thermal processing in the range of 380–600 °C has been thoroughly studied by a combined analysis of XANES and EXAFS spectra accompanied by electron microscopy examination. From changes in the Fe K-edge position valence state changes of Fe^{2+} ions, being due to a redox reaction that enables Ag^{+} ion reduction, have been deduced. The difference in the first Fe–O coordination sphere observed for the green glass and the iron oxide reference require further simulation of X-ray absorption spectra according to appropriate models of the oxygen environment of Fe in glass.

The relatively high concentration of Ag nanoparticles in glass samples of high Fe content resulted in EXAFS spectra being dominated by Ag–Ag correlations. From the temperature dependence of these spectra structural and thermodynamic parameters have been derived for samples of different mean size of Ag nanoparticles. Distinct size effects have been clearly confirmed for thermal expansion and lattice vibrations of the particles as well as their interatomic distances. A narrow size distribution achieved by reduced sample thickness and gradual thermal processing has been shown to make these effects more evident. Such configurations are well suited to explore thermoelastic

models which may predict the influence of the glass matrix on the material characteristics studied here. These results demonstrate that the EXAFS data of interatomic distances represent a sensitive tool for investigations of size and interface effects in nanocrystalline materials.

Acknowledgement

This work has been supported by Deutsche Forschungsgemeinschaft (SFB 418).

References

[1] F. Gonella, P. Mazzoldi, in: H.S. Nalwa (Ed.), Handbook of Nanostructured Materials and Nanotechnology, Vol. 1, Academic, 2000, p. 81.
[2] G. Mie, Ann. Phys. (Leipzig) 25 (1908) 377.
[3] U. Kreibig, M. Vollmer, in: Optical Properties of Metal Clusters, Springer Series in Materials Science, Vol. 25, Springer, Berlin, 1995.
[4] R.F. Haglund Jr., in: R.E. Hummel, P. Wissmann (Eds.), Handbook of Optical Properties II: Optics of Small Particles, Interfaces, and Surfaces, Vol. 2, CRC, New York, 1997, p. 191.
[5] F. Hacke, D. Ricard, C. Flytzanis, J. Opt. Soc. Am. B 3 (1986) 1647.
[6] R.V. Ramaswamy, H.C. Cheng, R. Srivastava, Appl. Opt. 27 (1988) 1814.
[7] E.M. Vogel, J. Am. Ceram. Soc. 72 (1989) 719.
[8] S. Schmitt-Rink, D.A.B. Miller, D.S. Chemla, Phys. Rev. B 35 (1986) 8113.
[9] C.F. Flytzanis, F. Hache, M.C. Klein, D. Ricard, P. Roussignol, in: E. Wolf (Ed.), Progress in Optics, Vol. 29, Elsevier, New York, 1991, p. 321.
[10] A. Meldrum, L.A. Boatner, C.W. White, Nucl. Instrum. Meth. B 178 (2001) 7.
[11] A.L. Stepanov, D.E. Hole, P.D. Townsend, J. Non-Cryst. Solids 260 (1999) 65.
[12] A. Berger, K.J. Berg, H. Hofmeister, Z. Phys. D 20 (1991) 313.
[13] K.-J. Berg, A. Berger, H. Hofmeister, Z. Phys. D 20 (1991) 309.
[14] C. Mohr, M. Dubiel, H. Hofmeister, J. Phys.: Condens. Matter 13 (2001) 525.
[15] G. De Marchi, F. Caccavale, F. Gonella, G. Mattei, P. Mazzoldi, G. Battaglin, A. Quaranta, Appl. Phys. A 63 (1996) 403.
[16] D.P. Peters, C. Strohhoefer, M.L. Brongersma, J. Van der Elsken, A. Polman, Nucl. Instrum. Meth. B 168 (2000) 237.
[17] H. Hofmeister, S. Thiel, M. Dubiel, E. Schurig, Appl. Phys. Lett. 70 (1997) 1694.
[18] R.F. Haglund Jr., D.H. Osborne Jr., R.H. Magruder, C.W. White, R.A. Zuhr, P.D. Townsend, D.E. Hole, R.E. Leuchtner, Mater. Res. Soc. Symp. Proc. 354 (1995) 629.
[19] I. Tanahashi, M. Yoshida, Y. Manabe, T. Tohda, J. Mater. Res. 10 (1995) 362.
[20] G. De Marchi, A. Licciulli, C. Massaro, L. Tapfer, M. Catalano, G. Battaglin, C. Meneghini, P. Mazzoldi, J. Non-Cryst. Solids 194 (1996) 225.
[21] H. Hofmeister, M. Dubiel, H. Goj, S. Thiel, J. Microsc. (Oxford) 177 (1995) 331.
[22] E. Borsella, F. Gonella, P. Mazzoldi, A. Quaranta, G. Battaglin, R. Polloni, Chem. Phys. Lett. 284 (1998) 429.
[23] N.A. Sharaf, R.A. Condrate, A.A. Ahmed, Mater. Lett. 11 (1991) 115.
[24] P.W. Wang, L. Zhang, Y. Tao, C. Wang, J. Am. Ceram. Soc. 80 (1997) 2285.
[25] K. Fukumi, K. Kageyama, M. Satou, J. Mater. Res. 10 (1995) 2418.
[26] M. Dubiel, S. Brunsch, L. Tröger, J. Phys.: Condens. Matter 12 (2000) 4775.
[27] S.N. Houde-Walter, J.M. Inman, A.J. Dent, G.N. Greaves, J. Phys. Chem. 97 (1993) 9333.
[28] M. Dubiel, H. Hofmeister, E. Schurig, Recent Res. Dev. Appl. Phys. 1 (1998) 69.
[29] M. Dubiel, S. Brunsch, W. Seifert, H. Hofmeister, G.L. Tan, Eur. Phys. J. D 16 (2001) 229.
[30] M. Dubiel, C. Mohr, S. Brunsch, H. Hofmeister, EUREM 12, Brno, Czech Republic, July 2000, Proceedings, p. 375.
[31] M. Dubiel, S. Brunsch, L. Tröger, J. Synchrotron Rad. 8 (2001) 539.
[32] J.J. Rehr, R.C. Albers, Rev. Modern Phys. 72 (2000) 621.
[33] D.C. Koningsberger, R. Prins (Eds.), X-Ray Absorption: Principles, Applications, Techniques of EXAFS, SEXAS, and XANES, Wiley, New York, 1988.
[34] Y. Iwasawa (Ed.), X-ray Absorption Fine Structure for Catalysts and Surfaces, World Scientific, Singapore, 1996.
[35] L. Wenzel, D. Arvanitis, H. Rabus, T. Lederer, K. Baberschke, Phys. Rev. Lett. 64 (1990) 1765.
[36] S.I. Zabinsky, J.J. Rehr, A.L. Ankudinov, R.C. Albers, M.J. Eller, Phys. Rev. B 52 (1995) 2995.
[37] A.I. Frenkel, J.J. Rehr, Phys. Rev. B 48 (1993) 585.
[38] L. Tröger, T. Yokoyama, D. Arvanitis, T. Lederer, M. Tischer, K. Baberschke, Phys. Rev. B 49 (1994) 888.
[39] G.N. Greaves, in: D.R. Uhlmann, N.J. Kreidl (Eds.), Glass Science and Technology, Vol. 48, Academic, London, 1991, p. 1.
[40] A. Berger, J. Non-Cryst. Solids 151 (1992) 88.
[41] S. Brunsch, PhD thesis, Martin-Luther University of Halle-Wittenberg, 2000.
[42] Y.S. Touloukian, R.K. Kirby, R.E. Taylor, P.D. Desai, in: Thermophysical Properties of Matter, Vol. 12, Plenum, New York, 1975, p. 298.

[43] E.A. Stern, J. Physique Coll. VI 7 (C2) (1997) 137.
[44] G. Dalba, P. Fornassini, R. Grisenti, D. Pasqualini, D. Diop, F. Monti, Phys. Rev. B 58 (1998) 4793.
[45] G. Dalba, P. Fornassini, R. Grisenti, J. Purans, Phys. Rev. Lett. 82 (1995) 4240.
[46] E. Sevillano, M. Meuth, J.J. Rehr, Phys. Rev. B 20 (1979) 4908.
[47] M. Dubiel, S. Brunsch, U. Kolb, D. Gutwerk, H. Bertagnolli, J. Non-Cryst. Solids 220 (1997) 30.
[48] R. Araujo, Appl. Opt. 31 (1992) 5221.
[49] C.H. Booth, P.G. Allen, J.J. Bucher, et al., J. Mater. Res. 14 (1999) 2628.
[50] K.-J. Berg, G. Berg, R. Gräbe, 66. Glastechn. Tagung, Fulda, Proc., May, 1992, p. 37.
[51] K.-D. Schicke, H. Hofmeister, M. Dubiel, Proc. Autumn School Mat. Sci. & Electron Microsc., Berlin 2002. Available from <http://crysta.physik.hu-berlin.de/as2002/posters.html>.
[52] T. Yokoyama, S. Kimoto, T. Ohta, Jpn. J. Appl. Phys. 28 (1989) 851.
[53] N. Miyata, H. Jinno, J. Mater. Sci. 16 (1981) 2205.
[54] Kaye and Laby, Tables of Physical and Chemical Constants, 16th Ed., G.W.C. Kaye and T.H. Laby, LONGMAN, 1995, P.72.
[55] C.W. Mays, J.S. Vermaak, D. Kuhlmann-Wilsdorf, Surf. Sci. 12 (1968) 134.
[56] F. Baletto, C. Mottet, R. Ferrando, Eur. Phys. J. D 16 (2001) 25.